Dye-loaded polymeric nanorods as bright fluorescent nano-platforms for efficient cellular uptake and bioimaging

Remi Pelletier, Anila Hoskere Ashoka, Deep Biswas, Elisabete Cruz da Silva, Andrey Klymchenko

Dye-loaded polymeric nanorods as bright fluorescent nano-platforms for efficient cellular uptake and bioimaging

Rémi Pelletier, Anila Hoskere Ashoka, Deep S. Biswas, Elisabete Cruz Da Silva, Andrey S. Klymchenko*

Laboratoire de Bioimagerie et Pathologies, UMR 7021 CNRS, Faculté de Pharmacie, Université de Strasbourg, Illkirch, France

*Email: andrey.klymchenko@unistra.fr

Abstract

Fluorescent dye-loaded polymeric nanoparticles have been extensively developed for cellular imaging as they are bright and versatile tools with large choice of polymers, dyes and surface chemistry. Here, we report preparation of fluorescent polymeric nanomaterials with high aspect ratio – nanorods, and study their cellular uptake for bioimaging applications. Fluorescent polymeric nanorods are prepared by scission of electrospun nanofibers using ultrasonication. To achieve high brightness, they are loaded with cationic fluorescent dyes (rhodamine or cyanines) with bulky hydrophobic counterions that prevent aggregation-caused quenching. The obtained nanorods of 400 nm diameter and 2-4 µm length show good fluorescence quantum yields (40% at 5% dye loading) and 800-fold higher brightness compared to 60-nm polymeric nanoparticles. Cellular studies reveal several remarkable features of nanorods vs NPs. First, nanorods internalization depends on the cell type, which was not the case of NPs. Second, we found that internalization of nanorods is nearly 100-fold more efficient than that of polymeric NPs, reaching ~3 wt% of the cell mass. The internalization of nanorods is an active process (endocytosis), which is inhibited by low temperature, absence of growth medium or nanorods treatment by a non-ionic surfactant. Despite this efficient internalization, nanorods exhibit negligible cytotoxicity according to three different types of assays. Due to high accumulation inside the cells, the labelled cells present ~100-fold higher fluorescence signal vs NPs, which remains for at least 6 days. This exceptional cell brightness enables single-cell tracking in two near-infrared spectral regions under the chicken skin. This work reveals exceptional capacity of polymeric nanorods to accumulate inside the cells, which allows efficient fluorescence labelling of cells for robust imaging and long-term tracking.

Graphical abstract

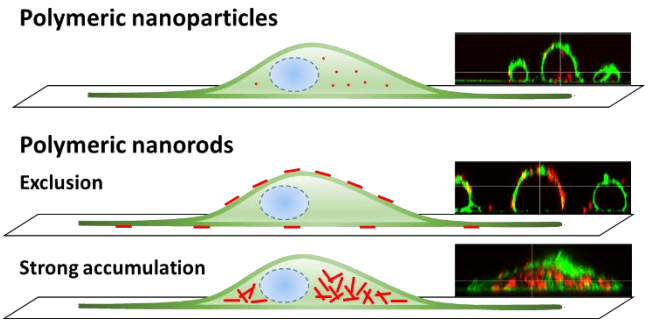

Introduction

Size and shape of nanomaterials have a profound effect of interaction with live cells and further cellular uptake.[1-2] It concerns in particular 1D nanomaterials,[3] particularly nanorods, which present unique behavior in biological systems due to high aspect ratio. [1-2,4] Nevertheless, literature reports provide contrasting picture on the effect of nanorod shape on the cell internalization. Thus, seminal works on gold nanorods modified with transferrin showed their slower internalization compared to spherical nanoparticles (NPs).[4] This conclusion was supported by a more recent study on gold nanorods.[5] Slow internalization of high aspect ratio nanomaterials inside the cells was also observed from nanofilaments made of block-copolymers[6] and cerium oxide nanorods.[7] Other studies of nanorods made the opposite conclusion. Thus, organic nanorods build of AIE dyes, coated with PEG-lipids showed increased uptake in certain cell lines.[8] Nanorod-shaped drug crystals showed a some increase in the cell uptake compared to spherical one, which improved drug action.[9] Mesoporous silica nanorods showed increased uptake but only for certain aspect ratio (2.1-2.5), while longer nanorods were less efficient.[10] Iron oxide nanorods also showed stronger internalization, but the effect was limited with only 1.2-1.4-fold enhancement.[11] Another interesting aspect is that nanorods may internalize differently into different cell lines. In addition to already mentioned reports on nanorods of AIE-based dyes,[8] mesoporous silica nanorods showed some specific uptake into cancer cells.[12] Another study suggested that rod-shape of nanostructures functionalized with antibodies, can improve specificity of uptake to specific cell lines.[13]

As a general tendency, synthesis of nanorods is easier for inorganic materials than for organic ones. Synthesis of soft polymeric nanomaterials of high aspect ratio is particularly challenging and, hence, the studies of their biological behavior are rather limited. The motivation to work on polymeric nanomaterials for nanomedicine is particularly high because they can be finely tuned in terms of their biocompatibility, biodegradability, capacity to encapsulate high amount of cargo and rich surface chemistry.[14-17] The existing methods for fabrication polymeric nanorods include photolithography combined with microfluidics,[18] stretching of spherical polymeric nanoparticles,[19] and template molding,[20] these approaches generally suffer from tedious fabrication procedures and thus high cost. Simpler approaches include self-assembly of block co-polymers[6] and dyes/drugs in combination with surfactants.[8-9]

We considered an alternative strategy based on preparation of electrospinning, which enables production of nanofibers from a large variety of polymers and with a varied diameter.[21-22] Moreover, electrospinning enabled encapsulation of large variety of bioactive molecules and contrast agents, which is of key importance for biomedical applications,[22-23] such as controlled release,[24-25] wound dressing[26-27] and tissue engineering.[23,28-30] However, only a few reports showed electrospun nanofibers could be converted into short nanofibers (nanorods), notably using ultrasonication of polymeric nanofibers.[31-32] Importantly, this approach could lead to polymeric nanorods with diameters >100 nm and micrometer lengths, which is similar to the size of bacteria.[33] However, the interaction of nanofibers of these dimensions with cells have not been sufficiently explored as majority of works focused on nanorods with diameter and lengths below micrometer.

Encapsulation of fluorescent dyes inside polymeric nanomaterials enabled preparation of bright nanoparticles for a large scale of applications such as sensing and bioimaging.[34-36] However, high dye loading required to achieving high brightness[36] generally leads to aggregation caused quenching (ACQ). To address this issue a number of methods were developed, notably using aggregation induced emission (AIE), which yielded ultrabright fluorescent nanomaterials.[37-38] However, this method is more suitable for preparation of nanostructures where the core of dye aggregates is coated with a polymer shell,[34] rather than dispersion of the dye in the polymer matrix.[39] The use of bulky side groups could also improve the brightness of polymeric materials, although this approach requires dedicated multi-step synthesis of rather complex dyes.[40] Previously, we proposed to use bulky counterions to prevent ACQ in polymer matrixes.[41] This method enabled high dye loadings inside polymeric NPs, yielding NPs of exceptional brightness[42] and light-harvesting properties.[43] They were successfully applied for amplified detection of nucleic acids[44-45] and oxygen[46] as well

as for long term cell tracking[47] and *in vivo* imaging at the single particle level.[48] More recently we showed that the counterion method could be applied to preparation of ultrabright electrospun nanofibers.[49] However, preparation of nanorods based on these bright polymeric materials have not been explored to date.

In this work, we developed a methodology of preparation of ultrabright fluorescent polymeric nanorods by ultrasonication of electrospun polymeric nanofibers loaded with dye/bulky counterion ion pairs. Their studies in cultures of five cell lines revealed several outstanding features of these high aspect ratio nanomaterials, such as stronger capacity to internalize inside the cells compared to NPs and some cell selectivity. Further studies confirmed that the nanofibers internalize by endocytosis and remained trapped in hypertrophic lysosomes. More importantly, quantitative internalization analysis by two independent methods revealed these polymeric nanorods exhibited nearly 100-fold stronger accumulation inside the cells compared to nanoparticles made of similar polymer. In U87 cells they were able to accumulate up to 3% mass of the cells, which is an outstanding amount of polymeric material inside the cells. Despite this exceptional accumulation nanorods showed no signs of cytotoxicity, verified by three independent methods. Finally, taking advantage of this strong accumulation, we applied polymeric nanofibers loaded with near-infrared dyes for single-cell detection under chicken skin at distance of ~2 mm.

Results and discussion

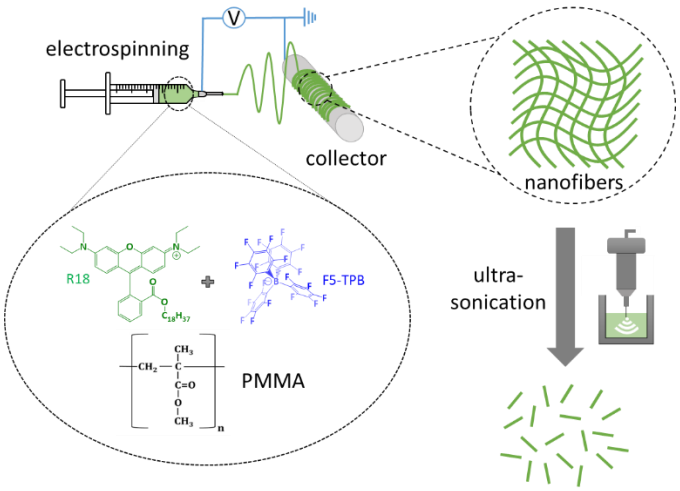

Figure 1. Preparation scheme for fluorescent dye-loaded polymeric nanorods.

Synthesis of fluorescent nanorods is based on dye-loaded polymeric nanofibers prepared by electrospinning method as we reported previously.[49] The nanofiber mats, loaded with 5 and 23 wt% (30 wt% ratio vs polymer mass) of R18/F5-TPB, were suspended in milliQ water and then sonicated with a probe sonicator (Figure 1). We observed that the initially heterogeneous suspension became homogeneous due to breaking of the long nanofibers into shorter nano-objects. Transmission electron microscopy (TEM) showed presence of short fibers with the thickness around ~0.4 µm and average length of 2-3 µm (Figure S1, Table S1). The former is close to the diameter of nanofibers in the fiber mats, reported by us before.[49] Thus, the sonication leads to breaking of the long fibers to shorter ones (nanorods). Even though there is some heterogeneity in the lengths of the fibers, we can notice that the fibers length for vast majority of nanorods was ≥ 1 µm. The latter implies that sonication can break nanofibers to rods but the process stops when the nanorod length reaches critical small size, below which the energy of sonication is not sufficient to break them. Nevertheless, there was no clear correlation between diameter and the length of individual nanorods, which was probably because the variation in the diameter was relatively small. Then, we studied optical properties by fluorescence spectroscopy. For both medium and high dye loading, namely 5 and 23 wt%, the emission

spectra were composed of a single emission band, similar to that for R18/F5-TPB dye loaded at 5 wt% into PMMA-MA NPs (Figures 2 and S2). The excitation spectra for 5 wt% loaded nanorods were nearly the same as for corresponding PMMA-MA NPs (Figures S2 and S3). High absolute quantum yields were observed both types of nanorods: 40 and 25%, respectively. In contrast, R18 with small inorganic perchlorate counterion showed poor emission and low fluorescence quantum yield (3%) already at 5 wt% dye loading, suggesting strong ACQ already at medium loading. These data are in line with our previous reports on nanofiber mats[49] and polymeric NPs,[41,50] where bulky counterion was found essential to prevent self-quenching of cationic rhodamine dye R18 by playing a role of spacer preventing formation of dye H-aggregates.[36]

Then, the nanorods were deposited on glass surface simply by sedimentation and studied by wide-field fluorescence microscopy. Nanorods were observed as fluorescence nanostructures with high aspect ratio (Figure 2). Their diameter could not be analyzed by this method because according to TEM it was close to the resolution of the optical microscopy (Table S1). However, the fact that the brightness of nanofibers was rather homogenous, we can conclude that the diameter of the obtained fibers should be also homogenous, in line with TEM results. Moreover, we observed quite good homogeneity of the length of the nanofibers for both dye loadings (Figures 2 and S4 and Table S2), with average length close to that obtained by TEM. The better homogeneity of length compared to TEM is probably related to the fact that sample preparation for fluorescence microscopy is much simpler, avoiding sample drying that lead to aggregation and inhomogeneous deposition on the surface. Therefore, we expect that the obtained distribution of lengths by fluorescence method reflects better the real state of the samples. We analyzed brightness of these nanorods in comparison with 60-nm PMMA-NPs. At the same experimental conditions, the signal detected from the center of nanorods was ~200-fold higher compared to NPs (Figure S5). This difference is clearly related to the much larger diameter of the nanorods, so that much larger number of dyes contribute to the signal for those larger nanostructures.[36]

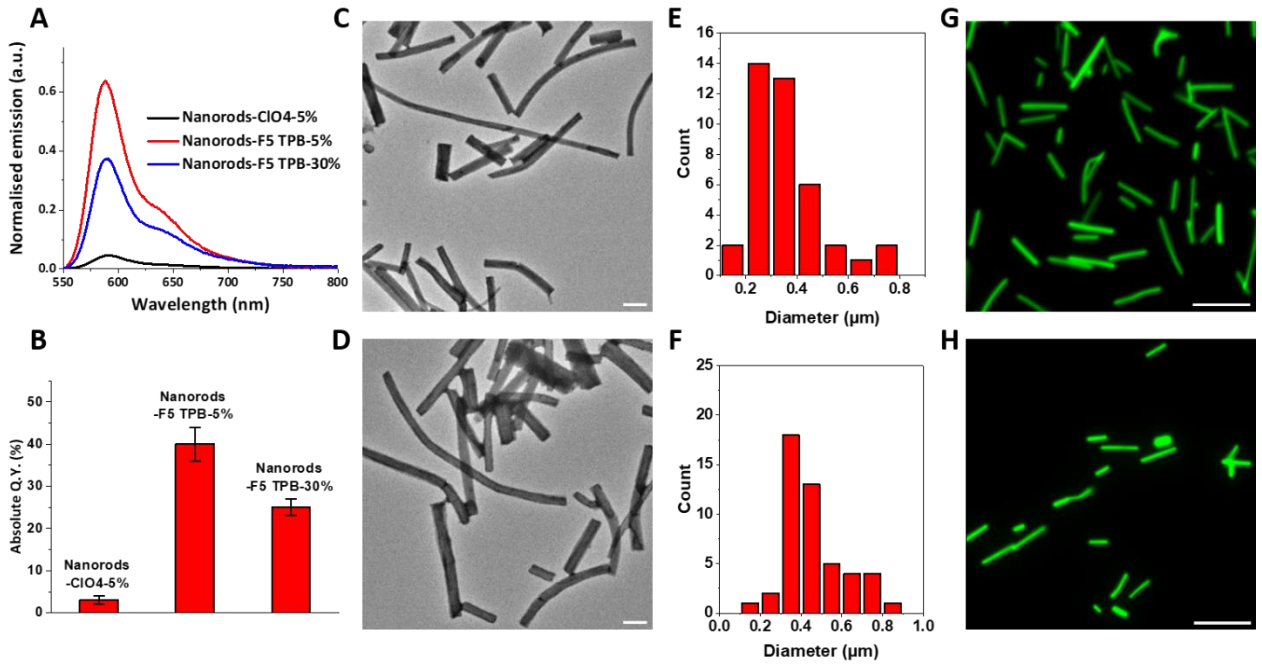

Figure 2. Physical characterization of fluorescent nanorods. (A) Fluorescence emission spectra of nanorods suspensions in water with various dye loading (resp. 5 wt% of R18 perchlorate salt or R18/F5-TPB salt and 23 wt% of R18/F5-TPB) normalized by corresponding absolute quantum yield. (B) Absolute quantum yield determined for corresponding nanorods suspensions. (C,D) TEM micrographs of nanorods loaded with 5 wt% (C) and 23 wt % (D) of R18/F5-TPB (with respect to the total mass). Nanorods were prepared from PMMA polymer. Scale bar 1 µm. (E,F) The thickness distribution of the nanorods. (G,H) Fluorescence microscopy images of fluorescent nanorods with 5 wt% (G) and 23 wt% (H) dye loading. Scale bar: 10 µm.

Then, we studied the interaction of nanorods with cells in comparison to fluorescent polymeric NPs made of similar polymer and loaded with the same dye R18/F5-TPB and loading degree (5 wt%). In case of NPs incubated with KB and U87 cells, we observed a perinuclear accumulation of the signal in the red channel (Figure 3), which according to our previous studies with this type of NPs corresponds to lysosomes. In sharp contrast, nanorods showed practically no internalization inside KB cells (Figure 3). A large fraction of nanorods could be found on the cell surface, as evidenced by colocalization with plasma membrane marker WGA-AF488. In case of U87 cells, the behavior was completely different as the cells presented strong intracellular fluorescence, where nanorods could be clearly identified by their morphology (Figure 3). However, there were practically no nanorods detectable on the cell surface. Due to sharp discrepancy in the behavior of nanorods in these two cells lines, we studied three additional cell lines: LNZ-308, EA.hy926 (EAHY) and HEK293T. In all three cell lines a strong signal of nanorods inside the cells was systematically observed (Figure S6), which indicates that nanorods tends to accumulate well inside the cells, while the behavior in KB cells is an exception. Thus, we can make two conclusions from this experiment. First, like NPs, nanorods internalized inside the cells. However, the inability of nanorods to enter KB cells remains a remarkable observation, which differ from NPs, indicating that nanorods could have a unique potential to distinguish some cell lines. The second conclusion is that the signal inside U87 was much higher compared to NPs, which suggests that for the same mass concentration outside the cells, the mass of nanorods (and the amount of encapsulated dyes) internalized inside the cells was much higher compared to that of NPs. Therefore, we explored further these two remarkable features of nanorods.

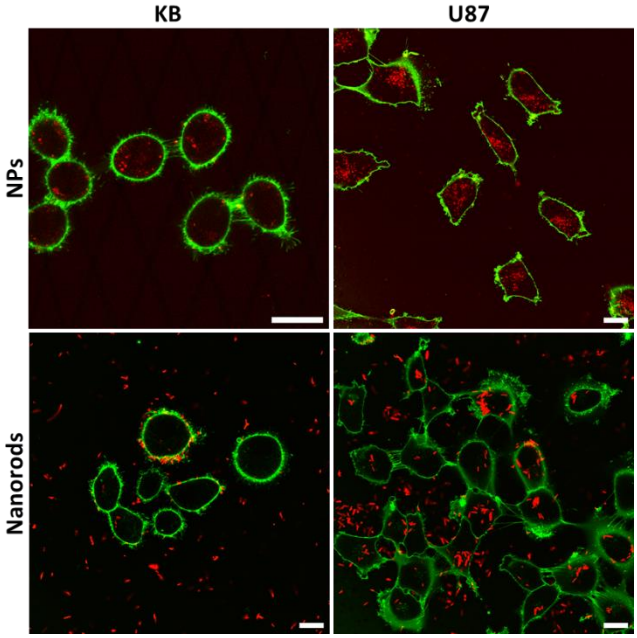

Figure 3. CLSM images of live cells (KB and U87) after 24h incubation in presence of fluorescent nano-objects (NPs and nanorods, shown in red). Plasma membrane was stained with WGA-AF488 before imaging (shown in green). Scale bar: 20 μm.

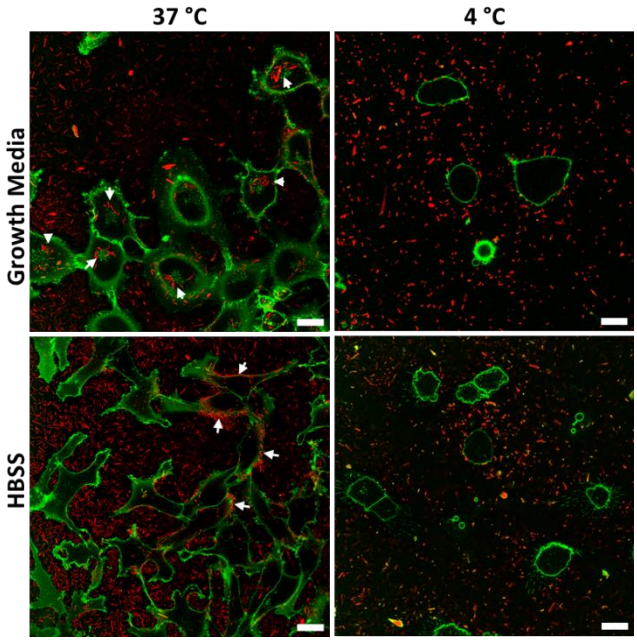

Figure 4. CLSM images of live U87 cells after 6h incubation in presence of fluorescent nanorods (shown in red) in complete growth medium and HBSS at 37°C and +4°C. Plasma membrane was stained with WGA-AF488 before imaging (shown in green). Scale bar: 20 µm. White arrows show internalized nanorods for growth media at 37 °C and cell-surface bond nanorods for HBSS at 37 °C.

To understand better the internalization of nanorods inside the cells, we studied the effect of low temperature (+4 °C), which is expected to block endocytosis. Moreover, we compared standard growth medium with physiological buffer HBSS. After 6h incubation in the standard growth medium, we could clearly observe internalization of nanorods inside U87 cells, whereas at +4 °C no sign of internalization was observed (Figure 4). This result suggests that nanorods enter the cells by active process (endocytosis) rather than by direct crossing of the plasma membrane. Remarkably, in HBSS medium, nanorods failed to enter cells: the majority of them remained on the glass surface, while some cells showed exclusively surface-bound nanorods (Figure 4). We can speculate that growth medium stimulates internalization probably due to adsorption of serum proteins on the surface of PMMA nanorods and the presence of growth factors. Previous report showed that unmodified nanorods may internalize differently because of protein corona.[51] Remarkably, when the nanorods were pretreated with Pluronic F127, the internalization inside U87 cells in complete growth medium was also inhibited (Figure S7). This implied that Pluronic F127 converts hydrophobic PMMA surface into hydrophilic “stealth” surface that prevents interaction with serum proteins with nanorods, thus inhibiting their internalization.

Then, the U87 and EAHY cells were incubated with nanorods for 6h and 24h and further co-stained with LysoTracker green and a membrane probe MemBright-640.[52] First, we noticed that nanorods attached to glass surface were labelled with MemBright-640 (Figure 5A), indicating that this amphiphilic probe directly interacts with nanorods, probably because of its hydrophobic interface. As MemBright-640 cannot really cross plasma membrane,[52] it could be used to distinguish the nanorods on the cells surface (positive staining with MemBright-640) from those inside the cells (not stained with MemBright-640). We found that at 6h incubation a significant amount of the nanorods were still co-localized with MemBright-640, indicating that a significant fraction of nanorods were bound to the cells surface (Figure 5A). However, after 24h, significant fraction of nanorods were observed without co-staining with MemBright-640 (Figure 5A), which implies that they entered the cells after this sufficiently long incubation time. Surprisingly, emission of nanorods was not co-localized at all with that of LysoTracker green (Figure 5A). To understand better this counter-intuitive

result, we incubated all 4 cells lines capable to internalize nanorods for 24h, and then, after their fixation and permeabilization, immunostaining of lysosomes was done by LAMP-3, while actin filaments were co-stained with phalloidine-AF488. Remarkably, we could observe colocalization of nanorods with LAMP-3 for all four cell lines (Figure 5B). Although we cannot exclude a slight cross-talk between the two channels, the merged images clearly show that nanorods outside the cells appear in red, while those inside the cells are systematically yellow due to LAMP-3 staining (Figure 5B). These results suggest that nanorods are trapped inside lysosomes. Then, the failure of LysoTracker green to stain lysosomes entrapping nanorods could probably originate from the incapacity of these hypertrophic compartments to generate sufficiently low pH, required for successful staining by LysoTracker green.

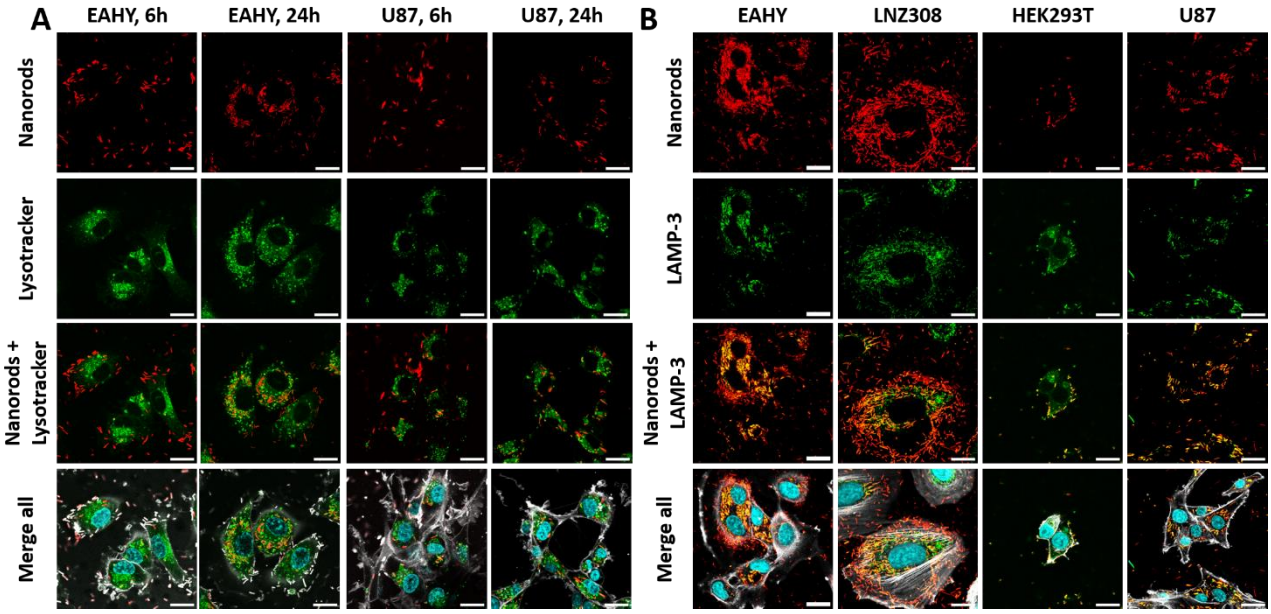

Figure 5. (A) CLSM images of live EAHY and U87 cells after 6h and 24h incubation in presence of fluorescent nanorods (shown in red). Plasma membrane was stained with MB647 (shown in grey), nucleus with hoechst 33342 (shown in cyan) and lysosomes with LysoTracker green (shown in green) before imaging. Scale bar: 20 µm. (B) CLSM images of fixed cells after 24h incubation in presence of fluorescent nanorods (shown in red). Actin was stained with phalloidin –AF488 conjugate (shown in grey), nucleus with hoechst 33342 (shown in cyan) and late endosomes with anti-lamp-3 primary antibody coupled with secondary AF647 conjugate antibody (shown in green). Scale bar: 20 µm.

As we observed a stronger accumulation of nanorods inside the cells compared to NPs, we wanted to make an absolute quantification of the internalized nanomaterial inside the cells. For this purpose, U87 cells were incubated for 24h with nanorods or NPs at the same mass concentration and then detached and fixed in suspension. One should note that the detachment of the cells by trypsinization also led to detachment of the non-internalized nanorods form the cell surface (data not shown). A set of meshes of 100 µm and 1 µm were used to separate cells from non-internalized nanorods or NPs. The cell concentration was determined by cell counting under microscope, where we could also clearly observe much stronger signal from cells incubated with nanorods compared to NPs (Figures 6, S8), in line with the initial microscopy observations (Figure 3). Then, the amount of fluorescent nanomaterials inside the cells was determined by absorbance measurement in organic solvent (1,4-dioxane) that solubilized the fluorescent dye. The measured absorbance value of 1 ml solution was 0.144 for nanorods per million cells counted, whereas for NPs this value was ~100-fold lower, namely 0.0014 (Figure 6D). These values correspond to 1.2 fmol and 11 amol of dyes per cell for nanorods and NPs, respectively. Considering the molar mass of the fluorophore and the dye loading used is a 5 wt%, it corresponds to 1.65 pg of dye and 33 pg of nanofibers per cell. Considering that the mass of a mammalian

cell is around 1-2 ng, the internalized nanorods presented 1.5-3 % of the mass of the cells. Thus, nanorods display impressively high capacity to internalize the cells, which is 100-fold higher than that of NPs.

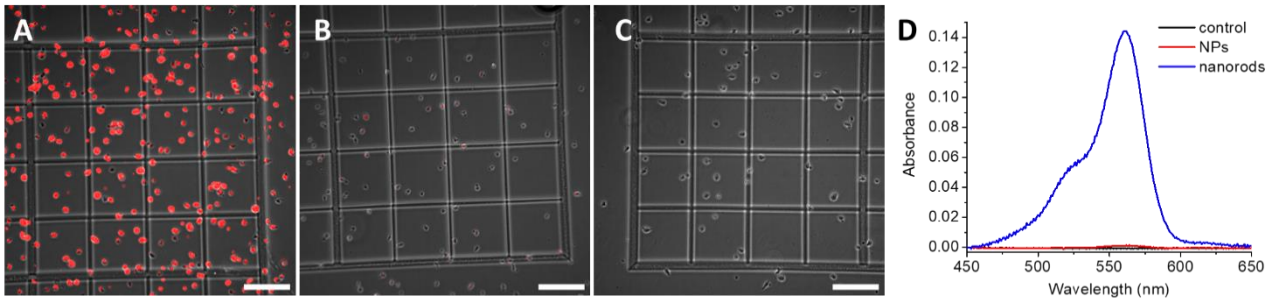

Figure 6. (A-C) Fixed U87 cells after 24h incubation with nanorods (A) or NPs (B) at 50µg/mL or non-treated (C) on counting slide before dissolving in 1,4-dioxane. Fluorescence channel is displayed at the same intensity for all samples. Scale bar: 200 µm. (D) Absorbance spectra of cellular lysates in 1,4-dioxane after 24h incubation with NPs or nanorods. Spectra are normalized according to the number of cells numbered for each sample.

Next, we made a quantitative analysis of the capacity of the five cells lines to internalize nanorods using flow cytometry in comparison to NPs. Four studied cell lines (U87, EAHY, LNZ308 and HEK293T) showed strong signal from the cells, where the signal from KB cells was relatively low (Figure 7), in line with our observations by fluorescence microscopy (see above). NPs incubated at the same conditions displayed nearly two order of magnitude lower signal (Figure 7), in line with our absolute quantitative analysis for U87 cells using absorption spectroscopy. Moreover, for all cells lines except KB, the signal from cells was higher compared to that of individual nanorods, suggested that multiple rods were present per cell in each line. As the signal from KB cells was between the control and individual nanofibers, we can conclude that nanorods were unable to enter KB cells, and the detected signal could be assigned to a fraction of small fragments of nanorods, which was probably present in the sample. Thus, multiple independent measurements, namely qualitative fluorescence microscopy, quantitative optical spectroscopy and flow cytometry show dramatic difference in the internalization of nanorods compared to NPs for the same mass concentration of the nanomaterials during incubation. This highlights the unique property of nano-objects with high aspect ratio to accumulate inside the cells. We also cannot exclude that larger size/mass of nanorods compared to NPs also contributed to their higher internalization.

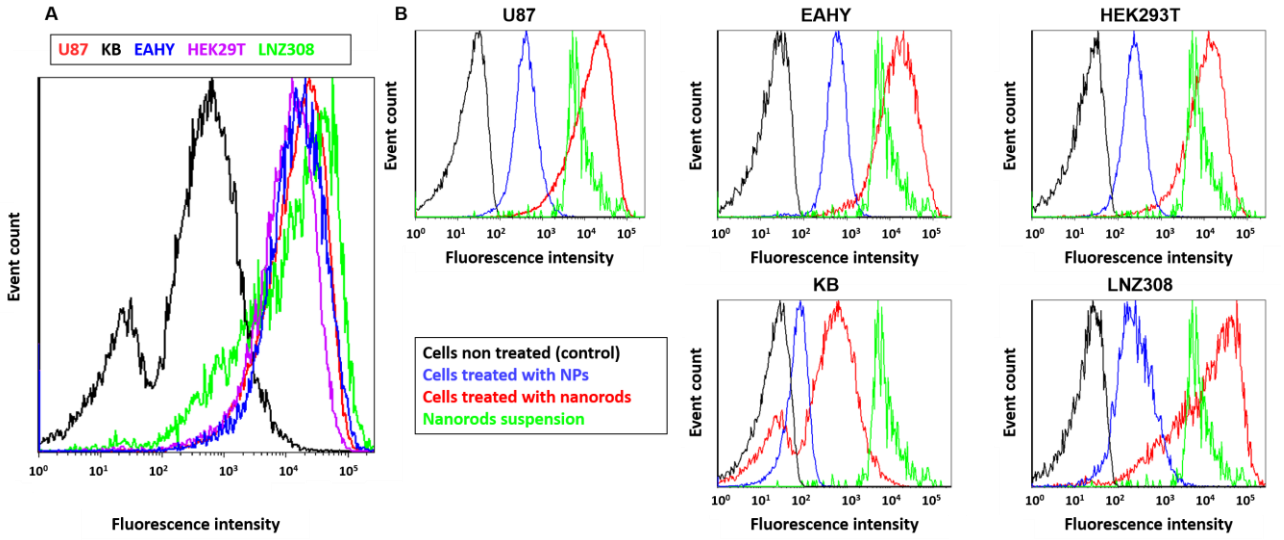

Figure 7. (A) Normalized to area fluorescent flow cytometry analysis (ex 561 nm, em 615/20 nm) of U87 , KB, EAHY, HEK293T and LNZ308, represented respectively in red, black, blue, purple and green lines, incubated 24h with 50 µg/mL nanorods. (B) Normalized to maximum fluorescent flow cytometry analysis (ex 561 nm, em 615/20 nm) of non treated control population of cells (in black), cells incubated 24h with 50 µg/mL of NPs (in blue) or 24h with 50 µg/mL of nanorods (in red) and a suspension of nanorods at 50 µg/mL in PBS with BSA (in green).

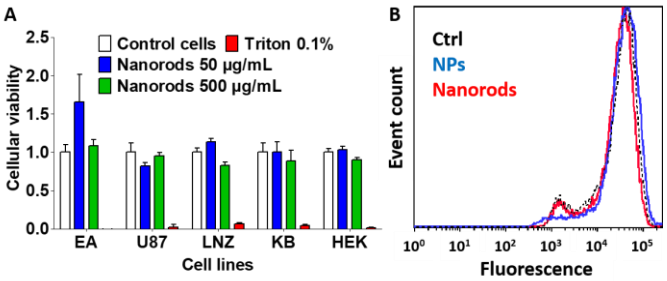

Figure 8. (A) MTT assay performed on 5 cell lines previously incubated 24h with nanorods at 50µg/mL and 500µg/mL. (B) Normalized to maximum fluorescent flow cytometry analysis (ex 488 nm, em 525/50 nm) of U87 cells stained with fluorescein diacetate 1h before analysis. Control cell (in black) and U87 cells incubated 24h with 50 µg/mL of NPs (in blue) or nanorods (in red).

This outstanding accumulation of nanorods required verification of their cytotoxicity. Therefore, MTT assay was performed, which estimates cytotoxicity through mitochondrial activity of cells. Remarkably, incubation of cells with nanorods for 24h resulted in no detectable cytotoxicity in comparison to control cells for all five cell lines tested (Figure 8A). Nanorods were not cytotoxic even at 500 µg/mL concentration, which corresponds to 50 times the concentration we used for microscopy experiments. In addition, we analyzed fluorescein diacetate labeling of U87 cells using flow cytometry, which is an alternative method to estimate cell viability, using intracellular esterase activity. Importantly, nanorods and NPs produced no change in the fluorescein signal compared to control cells (Figures 8B), indicating no sign of cytotoxicity of these two nanomaterials. Fluorescence microscopy imaging of multiple cells lines confirmed no effect of internalized nanorods on the intracellular signal of enzymatically cleaved fluorescein diacetate (Figure S9). Moreover, the cells with internalized nanorods detached by standard trypsin treatment were able to adhere on a new surface and continue to grow and divide at same rate as the non-treated control cells (Figure S10A), so their

key main biological functions were maintained. In addition, in these experiments, when cells were stained by trypan blue for automated counting, the rates of live cells were in the typical range of non-treated cells (eg. between 85 to 100 % for U87 cell line, Figure S10B), confirming the negligible toxicity and the maintenance of ATP related mechanism. Overall, nanorods despite their exceptional accumulation inside the cells are not cytotoxic, which could be explained by the fact that they are entrapped inside endosomes and thus do not interfere with biomolecular processes inside the cytosol. Importantly, after 3 and even 6 days of incubation, the strong signal from nanorods was still detected inside the cells (Figure S10C), suggesting that the nanorods remain inside the cells for prolonged time, allowing long-term imaging.

This strong accumulation of nanorods could be used to label the cells with high quantity of a contrast agent in order to identify the cells in a complex media. Here, we explored a possibility to detect cells labelled with nanorods under model tissue – chicken skin. To ensure deeper tissue penetration, we prepared nanorods loaded with near-infrared dyes hydrophobic derivatives of Cy5.5 and Cy7.5 with bulky counterion F5-TPB. The obtained nanorods showed similar structural characteristics as their rhodamine analogues (Figure S1, Table S1). Fluorescence spectra displayed emission bands typical for Cy5.5 and Cy7.5 dyes, with maxima centered at 720 nm and 835 nm, respectively (Figure S2B,C). Then, we incubated nanorods of two different colors independently in two populations of U87 cells for 24h. After trypsinization, these two cultures were mixed together and grown a glass coverslip for another 24h. Under fluorescent microscope, using two near-infrared channels for Cy5.5 and Cy7.5 dyes, the obtained co-culture appeared as two cell populations with strong signal in the green (Cy5.5 channel) and red (Cy7.5) channels (Figure 9A). The individual green- and red-colored cells could be clearly identified in a merged image together with a bright field channel. Then, the coverslip was covered by a freshly cut piece of chicken thigh skin, with a thickness of ~2 mm according to literature,[53-54] and imaged using the same fluorescence microscopy settings. Remarkably, the individual green and red signals could be identified directly under the chicken skin, suggesting that we could detect individual cells (Figures 9 and S11). The yellow signal, which was generally of higher intensity, could be assigned to cell aggregates combining cells of two populations of different emission color. Thus, due to capacity of nanorods to internalize into cells at high quantities, individual cells could produce strong emission signal in the two near-infrared regions. This enabled us to detect single cells in two colors under skin through ~2 mm, using basic epi-fluorescence setup with 10x objective.

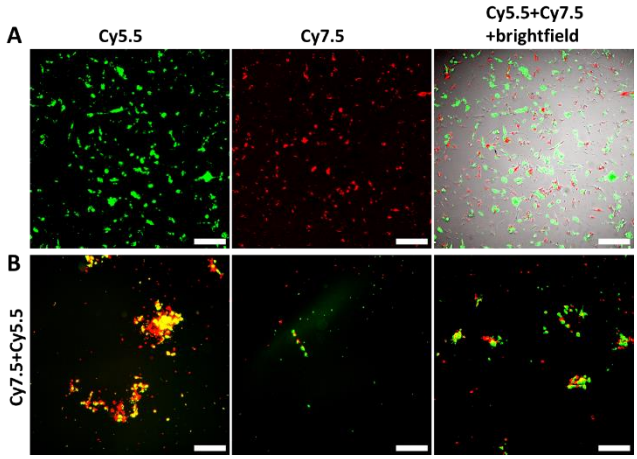

Figure 9. (A) Wide field images of a co-culture of two U87 cells batches incubated respectively with nanorods loaded with 5wt% Cy5.5/5-FTPB and nanorods loaded with 1wt% Cy7.5 TPB. (B) Similar co-cultured U87 cells microscopy images through chicken skin. Scale: 200 µm.

Conclusion

Understanding the role of aspect ratio in nanomaterials for interactions with the cells is a subject of intensive research. Here, we report preparation of fluorescent polymeric nanomaterials nanorods, and study their cellular uptake for bioimaging applications. We obtained them by scission electrospun polymeric nanofibers, loaded with cationic fluorescent dyes (rhodamine or cyanines) with bulky hydrophobic counterions. The latter prevents aggregation-caused quenching dyes in the polymeric matrix and thus ensure high fluorescence brightness. The obtained nanorods of 400 nm diameter and 2-4 μm length showed good fluorescence quantum yields: 40 and 23% at 5 and 30% dye loading. Fluorescence microscopy revealed 800-fold higher brightness of nanorods compared to 60-nm polymeric nanoparticles. Cellular studies highlighted dramatic differences in behavior of nanorods vs NPs. Unlike NPs, nanorods internalization depended on the cell type: while one cell line showed practically no internalization of nanorods, four others showed strong internalization. Moreover, fluorescence microscopy suggested much higher signal inside the cells for nanorods compared to NPs incubated at the same mass concentration. Quantitative optical spectroscopy of homogenized cells and flow cytometry suggested that internalization of nanorods is nearly 100-fold more efficient than that of polymeric NPs. The mass content of polymer inside the cells reached ~3 wt%, which is an exceptionally higher value. Fluorescence microscopy studies with immunostaning suggested that the internalization of nanorods takes place by endocytosis, which was confirmed by efficient inhibition of their internalization at low temperature. However, the absence of co-localization of nanorods with LysoTracker was interpreted as incapacity of the obtained hypertrophic endosomes to convert into mature lysosomes with low pH. Remarkably, nanorods were unable to enter the cells in simple buffers (like HBSS) without growth medium or after treatment by a non-ionic surfactant. These results highlight that surface properties and eventual adsorption of serum proteins could be crucial for their cell internalization. Despite the efficient internalization, nanorods showed negligible cytotoxicity according to three different types of assays: MTT, esterase activity and cell proliferation. High accumulation of ultrabright nanorods inside the cells resulted in exceptionally strong fluorescence labeling of the cells, where the signal was ~100-fold higher vs NPs. Moreover, the labelling of cells remained strong for at least 6 days. This unique property of nanorods was applied for single cell tracking in animal tissues, where strong fluorescence signal is particularly important. We showed that two cell populations labelled with nanorods operating in two near-infrared spectral regions (based on Cy5.5 and Cy7.5 dyes) could be tracked at the single cell level under the chicken skin ex vivo. Overall, we report preparation of fluorescent polymeric nanorods that exhibit exceptional capacity accumulate inside the cells. This allows highly efficient fluorescence labelling of cells that by far outperforms that of NPs, and thus opening the route for robust imaging and long-term tracking of cells in biological systems.

Material and methods

All of the chemicals and solvents were purchased from either Sigma Aldrich or TCI or Carlo Erba and used as received without further purification. MilliQ-water (Millipore) was used in all experiments. Fluorescence spectra were recorded on an Edinburg FS5 spectrofluorometer.

Electrospinning

The polymer solution for electrospinning was prepared by dissolving 500 mg of PMMA (25 wt %, Mw = 120 000) in 2 mL of DMF overnight. The resulting viscous solution was mixed with various concentrations of R18/F5-TPB and R18/ClO_4 (0.5−30 wt % with respect to the polymer concentration). The final concentration of the polymer in DMF was adjusted to 22 wt %. Electrospinning was performed on a FLUIDNATEK LE-10 electrospinning equipment (Bioinicia). Then, 1.5 mL of the above solution was loaded into a 5 mL syringe with a 18 G needle. A constant flow rate of 1.5 mL/h was maintained throughout with the help of a syringe pump. A voltage of 18 kV was applied to the syringe needle, and an aluminum foil was used as the collector. The

distance between the needle tip to the collector was adjusted to 15 cm. The fiber mat obtained after the electrospinning was dried in an oven at 80° C for 2 h. It was further dried under high vacuum overnight.

Nanorods preparation

Portions of electrospun fibermats were collected and weighted (typically around 10 mg). The fibers were soaked with a methanol/water mixture (40:60vol%) for 5 min and then washed two times with water. Then, fibers suspended in water were sonicated (Branson 150 sonicator probe 4C15) for 2x6min at 60% power in continuous mode in an ice bath to avoid over heating of the samples. The resulting nanorods suspensions were washed 4 times with sterile DPBS under sterile conditions to remove traces of fluorescent dyes that leaked during sonication. The sonication seems powerful enough to kill most of microorganisms. If handled in sterile conditions after sonication, no contaminations of cellular samples have been observed during this study. For pluronic F127 treatment, nanorods were centrifuged and resuspended in a pluronic solution in water below CMC value (0.5 mg/mL). After 1 h at 25 °C, 300 rpm in a thermoshaker excess of pluronic was removed by short centrifugation to resuspend nanorods in DPBS. Absolute quantum yields of the electrospun nanofibers were determined using an integration sphere (SC-30 Module, Edinburg Instruments). Transmission electron microscopy has been performed by the electron microscopy platform of IGBMC on a Tecnai F20 (200 kV FEG) system with negative staining from uranyl acetate.

Cell Lines, Culture Conditions and treatment

Cells were counted using Biorad TC20 Automated Cell Counter combined with a trypan blue exclusion assay to determine viability. Number of cells mentioned hereinafter correspond to live cells counted otherwise stated. U-87 MG (ATCC HTB-14), KB (ATCC CRL-3596) cells were grown in Eagle's Minimum essential medium (EMEM, Gibco Invitrogen), supplemented with 10% fetal bovine serum (FBS, Lonza), 2 mM L-glutamine (Gibco-Invitrogen), 1% non-essential amino acid solution (Gibco-Invitrogen), sodium pyruvate 1 mmol/L and phenol red at 37 °C in a humidified 5% CO_2 atmosphere. HEK293T (ATCC CRL-3216), LNZ308 (CVCL_0394), EA.hy926 (ATCC CRL-2922) cells were grown in Dulbecco's Modified Eagle's Medium (DMEM) with supplemented with 10% fetal bovine serum (FBS, Lonza), L-Glutamine and phenol red at 37 °C in a humidified 5% CO_2 atmosphere. Cells were seeded onto a chambered coverglass (IBIDI) at a density of 5×10^4 cells/well 24 h before the microscopy measurement. For microscopy imaging, the attached live cells in IBIDI dishes were washed once with warm OptiMEM solution (OptiMEM , Gibco- Invitrogen); after that, 1 mL of a corresponding dye solution in HBSS was added and the cells were incubated for 5 min at room temperature. Then, the attached cells in IBIDI dishes were washed twice with HBSS before imaging.

Fluorescence labelling

Membright 647 (MB 647) labelling have been performed in OptiMEM by addition of 1 µL of MB647 solution in DMSO (100 µM) per mL of medium (final concentration 100 nM) and incubated at RT for 5 min before imaging. Lysotracker green (Invitrogen, thermofisher scientific) has been used according to supplier's protocol at 50 nM in OptiMEM with 5 min incubation time at room temperature before imaging. Hoechst 33342 (Invitrogen, thermofisher scientific) labelling has been performed at 1 µg/mL with 30 min incubation time in growth medium before applying other staining for live cells imaging or incubated with secondary antibodies for immunostaining experiments. Wheat Germ Agglutinin AlexaFluor conjugate labelling (WGA 488 or WGA 647, Invitrogen, Thermofisher Scientific) has been performed according to supplier's protocol in HBSS for 10 min at 37 °C at 5 µg/mL. For immunofluorescence staining, cells were incubated for 15 min with 4% (w/v) formaldehyde solution in phosphate-buffered saline (PBS) at room temperature. The fixative solution was removed and the cells were washed with PBS 3 times. Then, the cells were treated with 1 mL of 0.1% Tween-20 in PBS respectively for 10 min at room temperature. The permeabilization solution was removed and washed 3 times with PBS. Cells were blocked with 0.5 % solution of BSA in PBS for 2 h at room temperature. Then, primary antibody (H5C6 anti LAMP-3) solution in 0.5 % BSA in PBS has been added and

cells incubated at + 4 °C overnight. Primary antibody were washed 3 times with PBS and then secondary conjugated antibody (Invitrogen AlexaFluo 647 conjugated anti mice) has been added with additional phalloidine AF488 conjugate at 100 nM and Hoechst 33342 and incubated for 2 h at room temperature. Cells were washed 3 times with PBS before imaging.

Fluorescence microscopy

Confocal imaging of cells was performed on a Leica SPE or Leica TCS SP8 confocal microscope with HCX PL APO 63×/ 1.40 OIL CS2 objective and two 12-bit photomultipliers. The excitation light was provided by lasers of 488 nm, 552 nm, and 638 nm. Epifluorescence imaging was performed with a Nikon Ti-E inverted epi-fluorescence microscope, equipped with CFI Plan Apo × 60 oil (NA = 1.4) objective and a Hamamatsu Orca Flash 4 sCMOS camera. The images were recorded using NIS Elements. All the images were processed using ImageJ.

Flow Cytometry Analysis

U87 cells were seeded at a density in 1×10^6/well in a 6-well plate 24h before addition of nanorods or NPs in growth medium. Before flow cytometry analysis, adhesive cells were first stained with fluorescein diacetate and Hoechst 33342. Then, live cells were washed once with warm DPBS and then detached with trypsin-EDTA treatment for 5 min at 37 °C, centrifuged, and resuspended in 500 µL of a solution of BSA 1% in DPBS. This suspension was passed through a 50 µm nylon mesh filter and kept on ice until analysis. For the experiment, the cells were analyzed using a MACSQuant® VYB flow cytometer. The detectors were calibrated in by the light scattering and fluorescence using MACSQuant® fluorescent calibration beads.

Cell viability assay

The MTT assay was performed to calculate the toxicity of the probe in mammalian cells. Cells were seeded at $5x10^3$/well and grown in 96-well plates. After 24 h of seeding, the cells were treated with different concentrations (50 and 500 µg/mL) of the NRs, respectively, and incubated for 24 h at 37 °C and 5 % CO_2. At the end of this incubation, the medium was removed from all the wells, and the cells were incubated further in fresh growth medium supplemented with 0.5 mg mL^{-1} of MTT for 4 h. The medium containing MTT was then removed, after which DMSO was added to solubilize the formazan. The absorbance values were recorded using a TECAN Spark plate reader at 570 nm. The cell viability was calculated as the absorbance with respect to the positive control as a reference, in which the cells were treated with triton X-100 at 0.1%. The results presented here are a mean of 8 wells ± standard error. Esterase activity was tested by incubating cells for 30 min at 37 °C in growth medium supplemented with 1 µM of fluorescein diacetate before imaging or flow cytometry analysis. Cell proliferation has been evaluated by first seeding U87 cells in 6 well plates at $1x10^5$ cells per wells. After 24 h, nanorods has been added at 50 µg/mL concentration. Three days after seeding, grow medium has been refreshed. For every time points, 3 wells were detached with trypsin-EDTA treatment (5 min at 37 °C) and cells were numbered and they viability check by trypan blue counting on biorad TC20 automated counter.

Cell internalization

U87 cells were incubated 24 h in complete media in presence of NRs at a final concentration of 100 µg/mL. Then, cells were washed three times with a solution of DPBS containing 1% of BSA to remove most of the unbound NRs. Cells were treated with a solution of trypsin 1x in DPBS for 10 min at 37 °C. Suspended cells were washed twice with cold DPBS by centrifugation (5 min, 1300 rpm) before being fixed with PFA at 4 % in DPBS for 15 min at room temperature. PFA was removed by washing 3 times with DPBS by centrifugation (5 min, 1300 rpm). Large aggregates and eventual fibers were removed by filtrating cells over 100 µm pluriStrainer (pluriSelect) and free NRs detached from cells surfaces during trypsin treatment were removed using 1 µm pluriStrainer (pluriSelect). Before use, strainers were conditioned with DPBS with 1 % BSA. Isolated cells were concentrated by centrifugation (15 min, 1300 rpm) and splited in two equal samples. One

was centrifuged and suspended in 1 mL of DPBS and used for manual cell counting using FastRead-102 slides (Biosigma) under transmitted light microscope. The second one was used for the concentration of internalized fluorescent dye. Cells were centrifuged (5 min 1300 rpm) to remove the supernatant and the bottom was dissolved in 1,4-dioxane by vigorous shaking and 30 min sonication in ultrasound bath at 40 °C. Before measuring absorbance, samples were centrifuged (10 min 1500 rpm) to remove non soluble cellular fragments and limit scattering of the resulting solution.

Acknowledgments

This work was supported by SATT Conectus Maturation Grant Biosensing and Agence nationale de la recherche (ANR) grant ANR-19-CE09-0006. This work used the Integrated Structural Biology platform of the Strasbourg Instruct-ERIC center IGBMC-CBI supported by FRISBI (ANR-10-INBS-0005). We thank Corinne Crucifix that performed TEM imaging.

References

(1) Albanese, A.; Tang, P. S.; Chan, W. C. The Effect of Nanoparticle Size, Shape, and Surface Chemistry on Biological Systems. *Annu Rev Biomed Eng* **2012**, *14*, 1-16.
(2) Makvandi, P.; Zarepour, A.; Zheng, X. Q.; Agarwal, T.; Ghomi, M.; Sartorius, R.; Zare, E. N.; Zarrabi, A.; Wu, A. M.; Maiti, T. K.; Smith, B. R.; Varma, R. S.; Tay, F. R.; Mattoli, V. Non-Spherical Nanostructures in Nanomedicine: From Noble Metal Nanorods to Transition Metal Dichalcogenide Nanosheets. *Applied Materials Today* **2021**, *24*.
(3) Shin, J.; Kang, N. Y.; Kim, B.; Hong, H. Y. S.; Yu, L.; Kim, J.; Kang, H. M.; Kim, J. S. One-Dimensional Nanomaterials for Cancer Therapy and Diagnosis. *Chemical Society Reviews* **2023**, *52*, 4488-4514.
(4) Chithrani, B. D.; Chan, W. C. Elucidating the Mechanism of Cellular Uptake and Removal of Protein-Coated Gold Nanoparticles of Different Sizes and Shapes. *Nano Lett* **2007**, *7*, 1542-1550.
(5) Yang, L. J.; Wang, J. H.; Sun, L. Y.; Zhang, Y. S.; Huang, P.; Guo, J. F. Comparison of Gold Nanospheres, Nanorods, Nanocages and Nanoflowers for Combined Photothermal-Radiotherapy of Cancer. *Nano* **2021**, *16*.
(6) Geng, Y.; Dalhaimer, P.; Cai, S.; Tsai, R.; Tewari, M.; Minko, T.; Discher, D. E. Shape Effects of Filaments Versus Spherical Particles in Flow and Drug Delivery. *Nat Nanotechnol* **2007**, *2*, 249-255.
(7) Chauhan, D.; Sri, S.; Kumar, R.; Panda, A. K.; Solanki, P. R. Evaluation of Size, Shape, and Charge Effect on the Biological Interaction and Cellular Uptake of Cerium Oxide Nanostructures. *Nanotechnology* **2021**, *32*.
(8) Feng, G.; Mao, D.; Liu, J.; Goh, C. C.; Ng, L. G.; Kong, D.; Tang, B. Z.; Liu, B. Polymeric Nanorods with Aggregation-Induced Emission Characteristics for Enhanced Cancer Targeting and Imaging. *Nanoscale* **2018**, *10*, 5869-5874.
(9) Li, W.; Zhang, X.; Hao, X.; Jie, J.; Tian, B.; Zhang, X. Shape Design of High Drug Payload Nanoparticles for More Effective Cancer Therapy. *Chemical Communications* **2013**, *49*, 10989-10991.
(10) Meng, H.; Yang, S.; Li, Z.; Xia, T.; Chen, J.; Ji, Z.; Zhang, H.; Wang, X.; Lin, S.; Huang, C.; Zhou, Z. H.; Zink, J. I.; Nel, A. E. Aspect Ratio Determines the Quantity of Mesoporous Silica Nanoparticle Uptake by a Small Gtpase-Dependent Macropinocytosis Mechanism. *ACS Nano* **2011**, *5*, 4434-4447.
(11) Thamizhchelvan, A. M.; Ma, H. D.; Wu, T. H.; Nguyen, D.; Padelford, J.; Whitworth, T. J.; Li, Y. C.; Yang, L. L. Y.; Mao, H. Shape-Dependent Cellular Uptake of Iron Oxide Nanorods: Mechanisms of Endocytosis and Implications on Cell Labeling and Cellular Delivery. *Nanoscale* **2024**.
(12) Cong, V. T.; Wang, W. Q.; Tilley, R. D.; Sharbeen, G.; Phillips, P. A.; Gaus, K.; Gooding, J. J. Can the Shape of Nanoparticles Enable the Targeting to Cancer Cells over Healthy Cells? *Advanced Functional Materials* **2021**, *31*.
(13) Barua, S.; Yoo, J.-W.; Kolhar, P.; Wakankar, A.; Gokarn, Y. R.; Mitragotri, S. Particle Shape Enhances Specificity of Antibody-Displaying Nanoparticles. *Proceedings of the National Academy of Sciences* **2013**, *110*, 3270-3275.

(14) Kamaly, N.; Xiao, Z. Y.; Valencia, P. M.; Radovic-Moreno, A. F.; Farokhzad, O. C. Targeted Polymeric Therapeutic Nanoparticles: Design, Development and Clinical Translation. *Chemical Society Reviews* **2012**, *41*, 2971-3010.
(15) Mitchell, M. J.; Billingsley, M. M.; Haley, R. M.; Wechsler, M. E.; Peppas, N. A.; Langer, R. Engineering Precision Nanoparticles for Drug Delivery. *Nature Reviews Drug Discovery* **2021**, *20*, 101-124.
(16) Elsabahy, M.; Wooley, K. L. Design of Polymeric Nanoparticles for Biomedical Delivery Applications. *Chemical Society Reviews* **2012**, *41*, 2545-2561.
(17) Vauthier, C.; Bouchemal, K. Methods for the Preparation and Manufacture of Polymeric Nanoparticles. *Pharmaceutical Research* **2009**, *26*, 1025-1058.
(18) Dendukuri, D.; Pregibon, D. C.; Collins, J.; Hatton, T. A.; Doyle, P. S. Continuous-Flow Lithography for High-Throughput Microparticle Synthesis. *Nat Mater* **2006**, *5*, 365-369.
(19) Champion, J. A.; Katare, Y. K.; Mitragotri, S. Making Polymeric Micro- and Nanoparticles of Complex Shapes. *Proceedings of the National Academy of Sciences* **2007**, *104*, 11901-11904.
(20) Rolland, J. P.; Maynor, B. W.; Euliss, L. E.; Exner, A. E.; Denison, G. M.; DeSimone, J. M. Direct Fabrication and Harvesting of Monodisperse, Shape-Specific Nanobiomaterials. *Journal of the American Chemical Society* **2005**, *127*, 10096-10100.
(21) Xue, J.; Wu, T.; Dai, Y.; Xia, Y. Electrospinning and Electrospun Nanofibers: Methods, Materials, and Applications. *Chemical Reviews* **2019**, *119*, 5298-5415.
(22) Xue, J.; Xie, J.; Liu, W.; Xia, Y. Electrospun Nanofibers: New Concepts, Materials, and Applications. *Accounts of Chemical Research* **2017**, *50*, 1976-1987.
(23) Goh, Y. F.; Shakir, I.; Hussain, R. Electrospun Fibers for Tissue Engineering, Drug Delivery, and Wound Dressing. *Journal of Materials Science* **2013**, *48*, 3027-3054.
(24) Luong-Van, E.; Grondahl, L.; Chua, K. N.; Leong, K. W.; Nurcombe, V.; Cool, S. M. Controlled Release of Heparin from Poly(E-Caprolactone) Electrospun Fibers. *Biomaterials* **2006**, *27*, 2042-2050.
(25) Chew, S. Y.; Wen, J.; Yim, E. K. F.; Leong, K. W. Sustained Release of Proteins from Electrospun Biodegradable Fibers. *Biomacromolecules* **2005**, *6*, 2017-2024.
(26) Rujitanaroj, P. O.; Pimpha, N.; Supaphol, P. Wound-Dressing Materials with Antibacterial Activity from Electrospun Gelatin Fiber Mats Containing Silver Nanoparticles. *Polymer* **2008**, *49*, 4723-4732.
(27) Azimi, B.; Maleki, H.; Zavagna, L.; De la Ossa, J. G.; Linari, S.; Lazzeri, A.; Danti, S. Bio-Based Electrospun Fibers for Wound Healing. *Journal of Functional Biomaterials* **2020**, *11*.
(28) Parham, S.; Kharazi, A. Z.; Bakhsheshi-Rad, H. R.; Ghayour, H.; Ismail, A. F.; Nur, H.; Berto, F. Electrospun Nano-Fibers for Biomedical and Tissue Engineering Applications: A Comprehensive Review. *Materials* **2020**, *13*.
(29) Yang, Y.; Xia, T.; Zhi, W.; Wei, L.; Weng, J.; Zhang, C.; Li, X. H. Promotion of Skin Regeneration in Diabetic Rats by Electrospun Core-Sheath Fibers Loaded with Basic Fibroblast Growth Factor. *Biomaterials* **2011**, *32*, 4243-4254.
(30) Li, M. Y.; Mondrinos, M. J.; Gandhi, M. R.; Ko, F. K.; Weiss, A. S.; Lelkes, P. I. Electrospun Protein Fibers as Matrices for Tissue Engineering. *Biomaterials* **2005**, *26*, 5999-6008.
(31) Sawawi, M.; Wang, T. Y.; Nisbet, D. R.; Simon, G. P. Scission of Electrospun Polymer Fibres by Ultrasonication. *Polymer* **2013**, *54*, 4237-4252.
(32) Niemczyk-Soczynska, B.; Dulnik, J.; Jeznach, O.; Kolbuk, D.; Sajkiewicz, P. Shortening of Electrospun Plla Fibers by Ultrasonication. *Micron* **2021**, *145*, 103066.
(33) Levin, P. A.; Angert, E. R. Small but Mighty: Cell Size and Bacteria. *Cold Spring Harb Perspect Biol* **2015**, *7*, a019216.
(34) Li, K.; Liu, B. Polymer-Encapsulated Organic Nanoparticles for Fluorescence and Photoacoustic Imaging. *Chemical Society Reviews* **2014**, *43*, 6570-6597.
(35) Reisch, A.; Klymchenko, A. S. Fluorescent Polymer Nanoparticles Based on Dyes: Seeking Brighter Tools for Bioimaging. *Small* **2016**, *12*, 1968-1992.
(36) Ashoka, A. H.; Aparin, I. O.; Reisch, A.; Klymchenko, A. S. Brightness of Fluorescent Organic Nanomaterials. *Chemical Society Reviews* **2023**, *52*, 4525-4548.
(37) Mei, J.; Leung, N. L.; Kwok, R. T.; Lam, J. W.; Tang, B. Z. Aggregation-Induced Emission: Together We Shine, United We Soar! *Chem Rev* **2015**, *115*, 11718-11940.

(38) Wang, H.; Li, Q.; Alam, P.; Bai, H.; Bhalla, V.; Bryce, M. R.; Cao, M.; Chen, C.; Chen, S.; Chen, X.; Chen, Y.; Chen, Z.; Dang, D.; Ding, D.; Ding, S.; Duo, Y.; Gao, M.; He, W.; He, X.; Hong, X.; Hong, Y.; Hu, J.-J.; Hu, R.; Huang, X.; James, T. D.; Jiang, X.; Konishi, G.-i.; Kwok, R. T. K.; Lam, J. W. Y.; Li, C.; Li, H.; Li, K.; Li, N.; Li, W.-J.; Li, Y.; Liang, X.-J.; Liang, Y.; Liu, B.; Liu, G.; Liu, X.; Lou, X.; Lou, X.-Y.; Luo, L.; McGonigal, P. R.; Mao, Z.-W.; Niu, G.; Owyong, T. C.; Pucci, A.; Qian, J.; Qin, A.; Qiu, Z.; Rogach, A. L.; Situ, B.; Tanaka, K.; Tang, Y.; Wang, B.; Wang, D.; Wang, J.; Wang, W.; Wang, W.-X.; Wang, W.-J.; Wang, X.; Wang, Y.-F.; Wu, S.; Wu, Y.; Xiong, Y.; Xu, R.; Yan, C.; Yan, S.; Yang, H.-B.; Yang, L.-L.; Yang, M.; Yang, Y.-W.; Yoon, J.; Zang, S.-Q.; Zhang, J.; Zhang, P.; Zhang, T.; Zhang, X.; Zhang, X.; Zhao, N.; Zhao, Z.; Zheng, J.; Zheng, L.; Zheng, Z.; Zhu, M.-Q.; Zhu, W.-H.; Zou, H.; Tang, B. Z. Aggregation-Induced Emission (Aie), Life and Health. *ACS Nano* **2023**, *17*, 14347-14405.
(39) Geng, J.; Li, K.; Qin, W.; Ma, L.; Gurzadyan, G. G.; Tang, B. Z.; Liu, B. Eccentric Loading of Fluorogen with Aggregation-Induced Emission in Plga Matrix Increases Nanoparticle Fluorescence Quantum Yield for Targeted Cellular Imaging. *Small* **2013**, *9*, 2012-2019.
(40) Zhang, B.; Soleimaninejad, H.; Jones, D. J.; White, J. M.; Ghiggino, K. P.; Smith, T. A.; Wong, W. W. H. Highly Fluorescent Molecularly Insulated Perylene Diimides: Effect of Concentration on Photophysical Properties. *Chemistry of Materials* **2017**, *29*, 8395-8403.
(41) Reisch, A.; Didier, P.; Richert, L.; Oncul, S.; Arntz, Y.; Mély, Y.; Klymchenko, A. S. Collective Fluorescence Switching of Counterion-Assembled Dyes in Polymer Nanoparticles. *Nature Communications* **2014**, *5*, 4089.
(42) Reisch, A.; Trofymchuk, K.; Runser, A.; Fleith, G.; Rawiso, M.; Klymchenko, A. S. Tailoring Fluorescence Brightness and Switching of Nanoparticles through Dye Organization in the Polymer Matrix. *ACS Appl Mater Interfaces* **2017**, *9*, 43030-43042.
(43) Trofymchuk, K.; Reisch, A.; Didier, P.; Fras, F.; Gilliot, P.; Mely, Y.; Klymchenko, A. S. Giant Light-Harvesting Nanoantenna for Single-Molecule Detection in Ambient Light. *Nature Photonics* **2017**, *11*, 657-663.
(44) Melnychuk, N.; Klymchenko, A. S. DNA-Functionalized Dye-Loaded Polymeric Nanoparticles: Ultrabright Fret Platform for Amplified Detection of Nucleic Acids. *Journal of the American Chemical Society* **2018**, *140*, 10856-10865.
(45) Melnychuk, N.; Egloff, S.; Runser, A.; Reisch, A.; Klymchenko, A. S. Light-Harvesting Nanoparticle Probes for Fret-Based Detection of Oligonucleotides with Single-Molecule Sensitivity. *Angewandte Chemie International Edition* **2020**, *59*, 6811-6818.
(46) Ashokkumar, P.; Adarsh, N.; Klymchenko, A. S. Ratiometric Nanoparticle Probe Based on Fret-Amplified Phosphorescence for Oxygen Sensing with Minimal Phototoxicity. *Small* **2020**, *16*, 2002494.
(47) Andreiuk, B.; Reisch, A.; Lindecker, M.; Follain, G.; Peyriéras, N.; Goetz, J. G.; Klymchenko, A. S. Fluorescent Polymer Nanoparticles for Cell Barcoding in Vitro and in Vivo. *Small* **2017**, *13*.
(48) Khalin, I.; Heimburger, D.; Melnychuk, N.; Collot, M.; Groschup, B.; Hellal, F.; Reisch, A.; Plesnila, N.; Klymchenko, A. S. Ultrabright Fluorescent Polymeric Nanoparticles with a Stealth Pluronic Shell for Live Tracking in the Mouse Brain. *ACS Nano* **2020**, *14*, 9755-9770.
(49) Ashoka, A. H.; Klymchenko, A. S. Ultrabright Fluorescent Polymeric Nanofibers and Coatings Based on Ionic Dye Insulation with Bulky Counterions. *ACS Appl Mater Interfaces* **2021**, *13*, 28889-28898.
(50) Andreiuk, B.; Reisch, A.; Bernhardt, E.; Klymchenko, A. S. Fighting Aggregation-Caused Quenching and Leakage of Dyes in Fluorescent Polymer Nanoparticles: Universal Role of Counterion. *Chemistry – An Asian Journal* **2019**, *14*, 836-846.
(51) Ge, F.; Xue, J. F.; Du, Y.; He, Y. Unmodified Single Nanoparticles Undergo a Motion-Pattern Transition on the Plasma Membrane before Cellular Uptake. *Nano Today* **2021**, *39*.
(52) Collot, M.; Ashokkumar, P.; Anton, H.; Boutant, E.; Faklaris, O.; Galli, T.; Mély, Y.; Danglot, L.; Klymchenko, A. S. Membright: A Family of Fluorescent Membrane Probes for Advanced Cellular Imaging and Neuroscience. *Cell Chemical Biology* **2019**, *26*, 600-614.e607.
(53) Cliche, S.; Amiot, J.; Avezard, C.; Gariepy, C. Extraction and Characterization of Collagen with or without Telopeptides from Chicken Skin. *Poultry Science* **2003**, *82*, 503-509.
(54) Christensen, K. D.; Zimmermann, N. G.; Wyatt, C. L.; Goodman, T. N.; Buhr, R. J.; Twining, P. Dietary and Environmental Factors Affecting Skin Strength in Broiler Chickens1. *Poultry Science* **1994**, *73*, 224-235.